Measurement and Modeling of Propagation Losses in Brick and Concrete Walls for the 900-MHz Band

Daniel Peña, Rodolfo Feick, *Senior Member, IEEE*, Hristo D. Hristov, *Senior Member, IEEE*, and Walter Grote

***Abstract*—The prediction of wall losses is a fundamental aspect in the planning of cellular systems. The broad variety of building materials and construction codes makes accurate attenuation prediction very difficult without the support of specific construction data or measurements. In this paper, the attenuation and equivalent electric parameters ε and σ of brick and doubly reinforced concrete walls are estimated for the 900-MHz band by fitting simple ray tracing models to empirical transmission data. The measurement setup is described, and extensive experimental results justifying the quasioptical modeling are presented.**

***Index Terms*—Materials parameters, measurements, modeling and simulation, RF propagation, RF system engineering.**

I. Introduction

MODELING of wave propagation through building walls has a significant impact on the planning of urban cellular telephone systems. The construction of walls is usually based on architectural and structural considerations, and even if the type of elements used is known, their influence on electromagnetic waves is difficult to predict. Rigorous analytical and numerical methods have been applied for studying models of nonhomogeneous building walls, but most of them have not been contrasted by measured data (for example, [1]–[3]). The computational requirements of these methods, when applied to professional design tools for complex indoor communication systems, are extremely high, and thus, their applicability in practice is still questionable. The through-wall propagation models presume that the configuration and construction materials are known in detail. Present-day indoor propagation software often use relatively simple models to describe the reflection and transmission by complex wall structures, offering the user the option of defining the electromagnetic wall parameters, [4]–[6]. As a whole, the investigations on the electromagnetic behavior of actual walls are rather scarce, and the reported results are likely to be applicable only to a specific type of wall. It is in general necessary to validate the applicability and accuracy of theoretical models by extensive empirical testing.

In this paper, the attenuation in brick and double reinforced concrete walls is studied. The latter wall types were of special interest to us because we were not aware of data for concrete walls with two reinforcing steel meshes. Such walls are sanctioned by the construction codes for some specific cases of building walls in countries with strong seismic activity, for example.

The paper centers on measurement procedures that do not require sophisticated test equipment and on the validation of a semi-empirical ray tracing modeling approach for finding the wall attenuation. It is proven initially that for the typical values of electric parameters ε and σ of a homogeneous wall and a frequency of 900 MHz, the transmitted wave is quasiuniform, and the use of classical ray tracing theory for studying reflection and transmission phenomena is well justified. The multi-ray model and its single-ray simplification for a lossy homogeneous wall are outlined briefly. For the latter, the mismatch attenuation is treated separately from the absorption attenuation. The numerical results show that the single-ray model works much better for transmission than for reflection. In the latter case, for thin and/or low loss walls, its use is not recommended. The main part of the paper is devoted to the description of empirical aspects and to the evaluation of models. This includes a description of the measurement setup, which is a noncoherent pulsed transmitter-receiver system that contrasts with more elaborate channel sounding systems and devices [7]–[10] employed for collecting and processing the experimental data. Validation of the theoretical models is based on verifying their ability to predict attenuation for a given type of building wall over a wide range of incidence angles. For this purpose, it is shown that the relevant equivalent parameters ε and σ of the model can be derived from simple measurements made for one or more walls representative of the type of construction under consideration. The evaluation of measurement data allows a comparison of the modeling accuracy for two types of walls: brick walls, which can be expected to meet the assumption of homogeneous behavior reasonably well, and double steel mesh reinforced concrete walls, which would be expected to significantly deviate from such behavior. The empirical data leads to the conclusion that in both cases, a very simple model allows good prediction of the through-wall attenuation.

II. Ray Modeling of Transmission Through Homogeneous Building Wall

We represent the wall as an infinite homogeneous flat plate with two electric parameters, relative permittivity $\varepsilon_r = \varepsilon/\varepsilon_0$ and conductivity σ, and thickness d. The following two ray-models are utilized for representing the wave reflection and transmission by the flat plate (see Fig. 1):

Manuscript received November 6, 2000; revised November 7, 2001. This work was supported by the Chilean National Science Agency CONICYT under Fondecyt Project 1010129.

D. Peña is with Siemens Chile, Santiago, Chile.

R. Feick, H. D. Hristov, and W. Grote are with the Department of Electronics, Universidad Tecnica Federico Santa Maria, Valparaiso, Chile (e-mail: chris@elo.utfsm.cl).

Digital Object Identifier 10.1109/TAP.2003.808539

a) multi-ray model, which takes into account the multiple reflection and refraction phenomena at the wall boundary planes [11], [12].
b) single-ray model for reflection (path $\boldsymbol{I}_1 - \boldsymbol{R}_1$) and for transmission (path $\boldsymbol{I}_1 - t - \boldsymbol{T}_1$).

According to the classical ray technique, at the boundary between two semi-infinite media, each uniform plane wave gives rise to one transmitted and one reflected uniform plane wave. For low-loss dielectric media, this assumption is accepted without discussion. However, in the case of a quasiconducting, homogeneous building wall, the transmission wave is converted into a nonuniform (hybrid) wave, and this requires the validity of ray tracing modeling to be justified. For the nonuniform wave a modified propagation constant $\gamma_m = \alpha_m + j\beta_m$ is defined, which differs from the intrinsic propagation constant $\gamma = \alpha + j\beta$. Here, α_m, α, and β_m, β are the corresponding attenuation and phase constants.

The modified constants α_m and β_m can be calculated using the following equations [13]:

$$\begin{pmatrix} \alpha_m \\ \beta_m \end{pmatrix} = \sqrt{\frac{1}{2}\left[\begin{bmatrix} +\mathrm{Re}(\gamma^2) \\ -\mathrm{Re}(\gamma^2) \end{bmatrix} + \beta_0^2 \sin^2\theta_i + \left|\beta_0^2 \sin^2\theta_i - \gamma^2\right|\right]} \tag{1}$$

with

$$\begin{pmatrix} \alpha \\ \beta \end{pmatrix} = \omega\sqrt{\mu_o\varepsilon_o\varepsilon_r}\sqrt{\frac{1}{2}\left[\begin{pmatrix} -1 \\ +1 \end{pmatrix} + \sqrt{1 + \left(\frac{\sigma}{\omega\varepsilon_o\varepsilon_r}\right)^2}\right]} \tag{2}$$

where $\beta_0 = \omega\sqrt{\varepsilon_0\mu_0}$ is the free-space wave number.

We first note that the limited thickness of any wall is not in agreement with the assumption of a semi-infinite medium, and thus, the conditions for the strict validity of (1) are not met. Our analysis at cellular frequencies, for thick lossy walls, for normal wave incidence have shown that the first reflection by the output boundary ($z = d$) contains less than 10% of the power transmitted through the input boundary ($z = 0$). This suggests that the effect of the interior reflections should not degrade considerably the accuracy of calculations that are based on the assumption of a semi-infinite wall, where such reflections do no exist. We next apply the theory of the nonuniform plane wave outlined above for checking the degree of wave nonuniformity in a lossy building wall. This was done numerically at 900 MHz by contrasting the values of the modified and intrinsic propagation constants α_m, β_m and α, β, respectively, for a concrete wall with measured parameters, $\varepsilon_r = 6.25$ and $\sigma = 0.037$ S/m [14]. It was found that for $\theta_i = 90°$, the maximum relative difference between the modified and intrinsic attenuation constant $[(\alpha_m - \alpha)/\alpha] \cdot 100$ (in percent) is quite small (about 7%), whereas the corresponding phase constant difference $[(\beta_m - \beta)/\beta] \cdot 100$ (in percent) is almost zero for all angles of incidence. Similar results have been obtained for a wall with parameters corresponding to brick wall: $\varepsilon_r = 4.6$ and $\sigma = 0.0175$ S/m [9], [10]. Therefore, it can be reasonably assumed that in walls with relatively small conductivity, the transmitted wave is practically uniform at typical mobile communications frequencies, and the use of the classical ray-tracing theory for studying reflection and transmission phenomena is well justified. In what follows, we use superscripts ($\perp$) or ($\|$) to specify the type of polarization, perpendicular (vertical), or parallel (horizontal), where necessary. The wave reflection and transmission coefficients at a boundary are marked by a subscript 1 (i.e., as R_1 and T_1) if the incident wave travels from air to wall and by a subscript 2 (i.e., as R_2 and T_2) if the wave travels from wall to air. These coefficients, which are usually referred to as Fresnel reflection and transmission coefficients, are found in classical texts on electromagnetics [15].

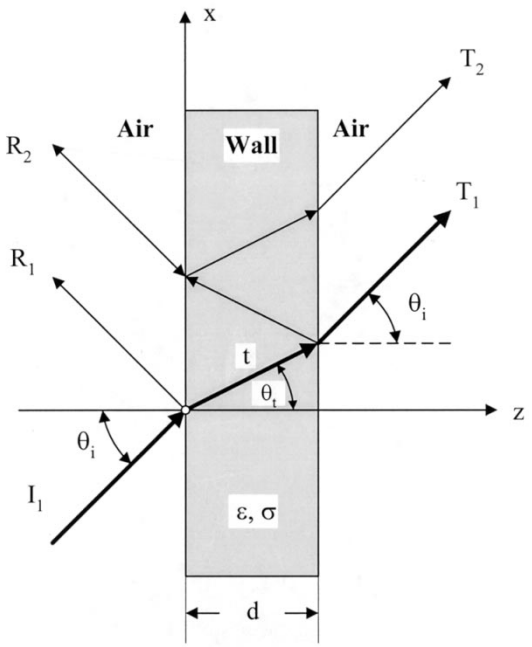

Fig. 1. Through-wall ray propagation models.

Normally, the multi-ray model of propagation is used for finding the total reflection and transmission coefficients R and T of a flat homogeneous wall. The equations for their calculation are given in [11] and [12], for example.

In the case of the single-ray transmission model, the amplitude reflection coefficient (which is designated as $\tilde{R}$) is equal to $|R_1|$. The amplitude transmission coefficient ($\tilde{T}$) can be expressed in the form

$$\tilde{T} = T_{12}A \tag{3}$$

where $T_{12} = |T_1T_2|$. The amplitude attenuation factor A, due only to the wall absorption losses along the inner transmission path t is given as an exponential attenuation function, or

$$A = e^{-\alpha t}. \tag{4}$$

In T_{12}, T_1 is the Fresnel transmission coefficient at the plane $z = 0$, equal to $T_1^{\perp}$ or $T_1^{\|}$, depending on the polarization; T_2 is the Fresnel transmission coefficient at the plane $z = d$, which is equal to $T_2^{\perp}$ or $T_2^{\|}$. Here, the coefficients T_1 and T_2 account for the attenuation due to the mismatch between air and wall media only or, equivalently, the attenuation, if the same wall is thought to be a lossless dielectric plate ($\sigma = 0$). For a lossless homogenous wall embedded in air, it is easy to derive the transmission

coefficient T_{12} for both polarizations, as a function of ε_r and θ_i, or

$$T_{12}^{\perp} = \left| \frac{4\cos\theta_i \sqrt{\varepsilon_r - \sin^2\theta_i}}{\left(\cos\theta_i + \sqrt{\varepsilon_r - \sin^2\theta_i}\right)^2} \right| \tag{5}$$

and

$$T_{12}^{\parallel} = \left| \frac{4\varepsilon_r \cos\theta_i \sqrt{\varepsilon_r - \sin^2\theta_i}}{\left(\varepsilon_r \cos\theta_i + \sqrt{\varepsilon_r - \sin^2\theta_i}\right)^2} \right|. \tag{6}$$

It is seen that in the single-ray model, the mismatch attenuation can be treated separately from the absorption attenuation. As we show later, this property can be very useful in practice for the empirical determination of the conductivity.

Examples of numerical comparisons between the multi-ray and single-ray models are shown in Figs. 2 and 3 for a wall of thickness 27 cm, frequency 890 MHz, and normal wave incidence. Fig. 2 illustrates the dependence of reflection and transmission coefficients on permittivity in a range from 2 to 12, with $\sigma = 0.05$ S/m as a parameter. It is seen that in the typically quoted range for $\varepsilon_r = 3$ to 9, the transmission coefficient varies by less than 3 dB. Fig. 3 shows the transmission and reflection coefficients versus conductivity for $\varepsilon_r = 6$. It is seen that the transmission coefficient changes by around 16 dB for the typical range of values for σ (0.01 to 0.1 S/m) quoted in the literature [8], [10], [18], [19].

Calculations of the transmission coefficient as a function of wall thickness, for different σ and ε_r as parameters, have also shown a small difference between the values predicted by the two models. For example, if $\sigma = 0.05$ S/m and $\varepsilon_r = 6$, and if the thickness ranges from 10 to 50 cm, the attenuation difference varies from 0.7 to 0.05 dB. For the thickness of 27 cm, it is about 0.1 dB.

Similar results have been obtained for oblique wave incidence and for other typical values of σ, ε_r, and d as parameters. The conclusion can be drawn that for brick and concrete walls, the single-ray model performs adequately for transmission, whereas for reflection the use of the more accurate multi-ray model would be more appropriate.

III. Modified Friis Equation and Measurement of Through-Wall Attenuation

As was shown in the previous section, in the case of typical brick and concrete walls, the simpler single-ray transmission model can be used without significant loss of accuracy in comparison to the multi-ray transmission model.

We next modify the Friis equation for a free-space wireless link in order to account for the through-wall power loss expressed by the power transmission coefficient T^2 (or $\tilde{T}^2$ in the case of the single – ray model). This equation is written here in logarithmic form in order to use standard decibel units, or

$$P_r(\text{dBm}) = P_t(\text{dBm}) + G_t(\text{dB}) + G_r(\text{dB}) + 20\log_{10} T - 20\log_{10} f(\text{MHz}) - 20\log_{10} r(\text{m}) + 27.6 \tag{7}$$

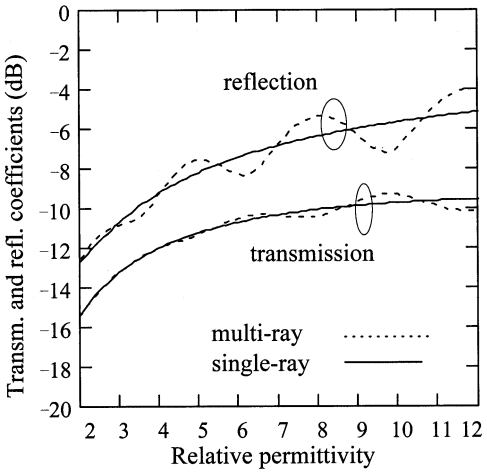

Fig. 2. Transmission and reflection coefficient versus permittivity.

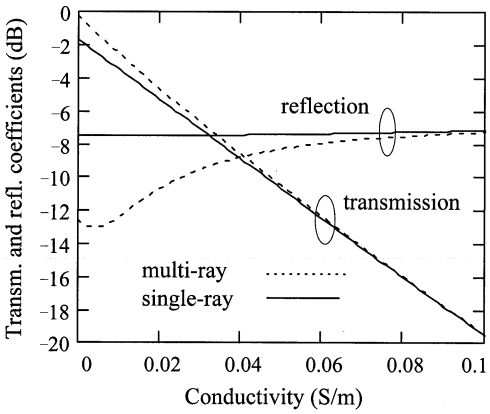

Fig. 3. Transmission and reflection coefficient versus conductivity.

where P_r and P_t are the powers at the receiver and transmitter antenna output and input; G_r and G_t are the receiver or transmitter antenna gain, respectively; and r is the distance between receiving and transmitting antenna, corresponding to line-of-sight distance in free space.

The measurement setup described in what follows is basically aimed at the determination of power attenuation for a range of angular positions. From this, the power transmission coefficient T^2 as a function of the incidence angle is determined, and the equivalent parameters ε_r and σ that best fit the measured attenuation versus angle curve are obtained.

We first note that the predicted attenuation can only be expected to reflect average values for any given real situation. In this sense, the basic assumption of a homogenous wall modeled by equivalent parameters corresponds to assuming that the deviations from this ideal condition can be treated as a random variable. Therefore, for each wall tested, multiple measurements were performed at various horizontal and vertical antenna positions for each angle of incidence to obtain average and deviation data. To simplify the measurement procedure, the transmitting and receiving antennas were kept at a constant distance from the wall. For a fixed transmitting position, the receiving antenna was moved on a path parallel to the wall. Thus, if for normal incidence the distance between transmitting and receiving antenna

is r_0, then for this setup, r is equal to $r_0/\cos\theta_i$. Here, the small error due to the change in propagation direction inside the wall is neglected. Practical considerations also limit the measurement range to angles of less than 70°.

To isolate the effect of multipath propagation signals, a wideband measurement system was implemented, based on the periodic transmission of very short RF pulses, demodulated at the receiver with a microwave detector. A pulse duration of 10 ns was used. At the frequencies of interest for cellular systems, the far-field condition is met at very short distances; therefore, the path length for the measurement link may be quite small. For the half-wave dipoles used as transmitting and receiving antennas, the far-field conditions are easily fulfilled for the minimum path length used: 1.3 m. Thus, free space loss can be kept small, and power/sensitivity requirements for the measurement system can be quite modest. The system used is described in Fig. 4. Standard commercial elements were used to build the transmitter and receiver. The detector power to voltage conversion characteristic was first determined, and the whole system was calibrated under free space propagation conditions prior to each measurement session. The input power at the transmitting antenna terminals P_t was 24 dBm, and the total receiver gain was adjusted according to specific conditions to avoid amplifier saturation and to keep the received power within the detector's operating range. To allow an easy comparison of the results, however, all power measurements as well as the values predicted by the theoretical models are specified at the detector terminals, after rescaling by the receiver gain of 37.2 dB. This implies modifying (7) to

$$P_{in}(\text{dBm}) = P_r(\text{dBm}) + 37.2. \tag{8}$$

The distance r_0 between transmitting and receiving antenna for normal incidence was chosen as 1.3 m, and the corresponding received power at the detector input P_{in} was 31 dBm under free space conditions. Comparison of this reference value with the plotted results allows the determination of total loss from transmission through wall. For the measurements with parallel polarization, where the dipole antenna pattern is not isotropic in the incidence plane, care was taken to always keep the aim of the antenna lobe aligned with the direction of measurement. For each wall, measurements were performed at 12 different antenna positions (four horizontal and three vertical), forming a rectangular mesh with 15 cm point spacing on average. For each of these positions, the incidence angle θ_i was varied between 0 and 70° in 2° increments. The exact positioning of the points was, however, varied randomly in a ±3 cm range to avoid any possibility of systematic errors due to a periodic structure of the wall. For any given angle θ_i, the average measured power $\overline{P}_{in}(\theta_i)$ was defined as the arithmetic average of all 12 measurements. This is the quantity to be compared with the input power $P_{in}(\theta_i)$ predicted by the theoretical model.

IV. Measurement Results and Modeling Accuracy

A. Model Fitting Criteria

The model adjustment procedure used consists of finding the combination of equivalent parameters ε_r and σ, which generates the theoretical curve of $P_{in}(\theta_i)$ versus θ_i that best fits the averaged measurement curve $\overline{P}_{in}(\theta_i)$. As a criterion for best fit, the minimization of the average r.m.s. error $e_{r.m.s}$ (over the angle of incidence θ_i) was chosen. We thus define

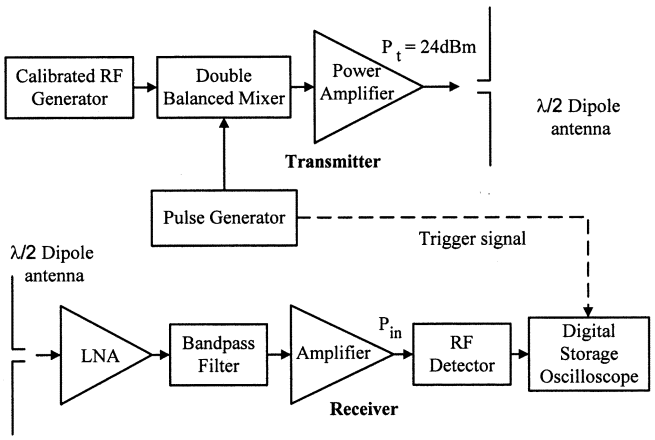

Fig. 4. Transmitter/receiver.

$$e_{r.m.s}(\text{dB}) = \sqrt{\frac{1}{N}\sum_{\theta_i}\left|\overline{P_{in}}(\theta_i),(\text{dBm}) - P_{in}(\theta_i),(\text{dBm})\right|^2} \quad \text{for } \theta_i = 0^\circ, 2^\circ, \ldots, 70^\circ \tag{9}$$

where N is the number of angular positions, which in our case is equal to 36.

As, for any given angle of incidence, the above r.m.s. error is based on an average of 12 measurements, the r.m.s. error as a function of the angle is also calculated. If $M_j(\theta_i)$ is the jth measurement at angle θ_i, the unbiased estimate of the r.m.s error $\Sigma(\theta_i)$ is defined as

$$\Sigma(\theta_i) = \sqrt{\frac{L\sum_{j=1}^{L} M_j(\theta_i)^2 - \left(\sum_{j=1}^{L} M_j(\theta_i)\right)^2}{L(L-1)}} \tag{10}$$

where $L = 12$.

For a given wall, $\Sigma(\theta_i)$ provides a useful insight into the deviation from the average behavior that can be expected at a given angle. If $\Sigma(\theta_i)$ is much larger than $e_{r.m.s.}$, then it can be concluded that large variations in propagation behavior can be expected, due to lack of homogeneity of the wall. It should be noted that $\Sigma(\theta_i)$ reflects variations with respect to the average of measurements and not with respect to the theoretical model.

B. Description of the Walls Tested

Two different types of walls were tested to verify the accuracy of the models.

1) *Brick walls:* These inside dividing walls are made of bricks and mortar and are covered by a layer of stucco. Two walls were tested: one of thickness 23 cm ("wall 1") and the other of thickness 17 cm ("wall 2"). The walls correspond to a construction more than 20 years old for which little architectural data is available.
2) *Steel reinforced concrete walls:* They correspond to a building of recent construction and detailed data was available. Two nominally identical interior walls ("wall 3" and "wall 4") were tested. They are made of concrete

and reinforced by two meshes of 8-mm-thick steel rods. The square meshes consist of horizontal and vertical rods, spaced 20 cm apart, and tied together with steel wire at the crossings. They lie at opposing sides of the wall, separated by 18 cm, as shown in Fig. 5. The meshes are not connected to each other but, as a result of the building procedures used, should have been aligned in the sense that a vector normal to the wall incident upon one rod will also be incident on the corresponding rod at the other side. The wall is covered by a 1–cm layer of stucco. Total thickness of the walls is 27 cm.

In the literature, data for solid concrete walls [3], [9], [17] or for walls reinforced by single steel grids of parallel rods or square-element meshes [6], [10], [14], [16], [18], [19] are usually quoted. We are not aware of data for concrete walls with two reinforcing steel meshes, which are similar to those studied in this work. Such walls are sanctioned by the construction codes in some specific cases (for example, in countries with a strong seismic activity).

For both types of walls, the measurements include perpendicular and parallel polarization. It should be noted that a total of close to 3500 individual power measurements were performed.

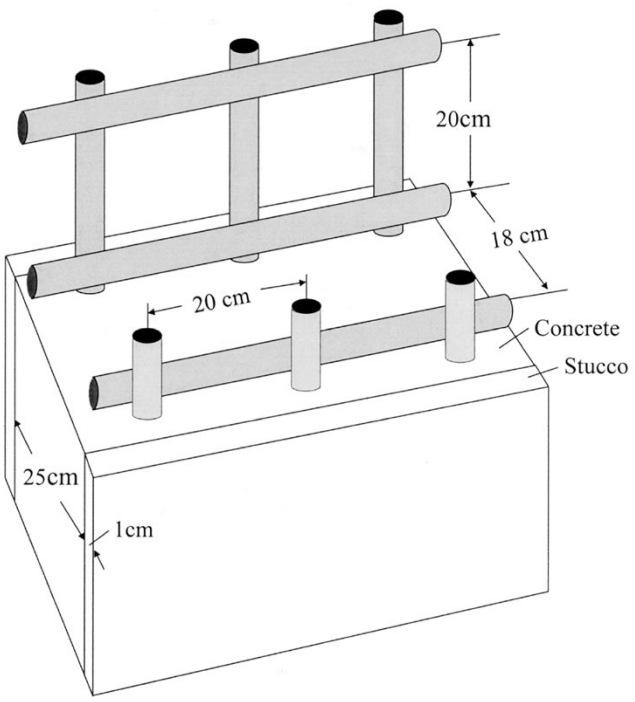

Fig. 5. Description of double reinforced concrete wall.

C. Modeling Results

We present here the more relevant results of our empirical work. The approach consist in fitting a theoretical model to the measurement results obtained for a given wall and then to determine the accuracy of this model when applied to the prediction of attenuation for a wall of nominally the same type of construction. As will be seen, in most cases, the models proved accurate enough for practical use. As will be discussed below, the homogeneity assumption is better met by brick walls than by steel-reinforced concrete walls. Fig. 6 shows the case of a brick wall 1 for perpendicular and parallel polarization. Since the curves produced by means of both theoretical models are virtually overlapping, only the curves corresponding to the single-ray model are shown in each case. As mentioned before, the received power at the detector would be 31 dBm for normal incidence and free space conditions. The values of the equivalent parameters, which result in the smallest r.m.s. error, were $\varepsilon_r = 4$ and $\sigma = 0.022$ S/m for perpendicular polarization and $\varepsilon_r = 4$ and $\sigma = 0.024$ for parallel polarization. The attenuation at normal incidence is 5.2 and 5.6 dB for perpendicular and parallel polarization, respectively. The similarity of the parameter values attests to the homogeneity of the brick wall.

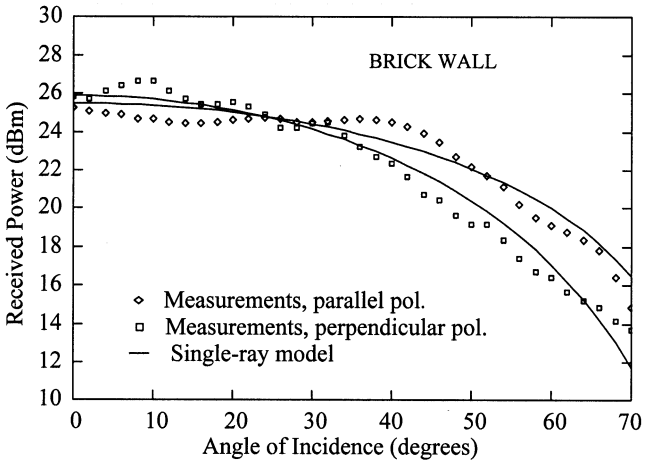

Fig. 6. Received power for brick wall (wall 1).

Table I shows values of ε_r and σ and the corresponding average r.m.s error as defined by (9). The measurements made for wall 1 were used for model fitting, and the corresponding r.m.s modeling error is shown. As can be seen, unambiguous determination of both ε_r and σ is not possible by this method. The r.m.s prediction error shown for wall 2 is obtained from (9) using the same equivalent parameters that were fit to wall 1. Reversing the procedure, i.e., using wall 2 for fitting equivalent parameters and then testing them on wall 1 yields similar accuracy. As discussed in Section III, the empirical data corresponds to multiple wall positions and incidence angles, and thus, the r.m.s. error obtained reflects the quality of the model fit and prediction for a very large average of measured values. It is observed that for the range of typical values of ε_r [8]–[10], the prediction model yields acceptable accuracy. The choice of values of σ is quite critical, and selecting a value that differs significantly from those shown in Table I leads to large modeling errors regardless of the value of ε_r. As was discussed in Section II, the wall transmission coefficient depends much more on conductivity than on permittivity, and thus, the above result was, of course, expected. It is also worth noting that, as was predicted by theory, both theoretical models (single-ray and multiple-ray) provide similar fit to the measured data over the whole angular range.

Fig. 7 illustrates the behavior of a steel reinforced concrete wall (wall 4) for perpendicular and parallel polarization. Bearing in mind that the theoretical maximum power at the detector would again have been 31 dBm without the wall, it is seen that attenuation is much larger than for the brick wall, which is a consequence mainly of the reinforcing elements.

TABLE I
MODELING ACCURACY FOR BRICK WALL

		Wall 1 (reference)				Wall 2 (prediction errors)	
		Perpendicular		Parallel		Perpendicular	Parallel
Model	ε_r	σ (S/m)	$e_{r.m.s}$ (dB)	σ (S/m)	$e_{r.m.s}$ (dB)	$e_{r.m.s}$ (dB)	$e_{r.m.s}$ (dB)
Single-ray	3	0.022	0.74	0.022	0.67	1.55	1.00
	4	0.022	0.73	0.024	0.65	1.68	0.95
	5	0.022	0.74	0.026	0.71	1.84	1.04
Multi-ray	3	0.022	0.86	0.022	0.65	2.01	1.09
	4	0.020	0.75	0.024	0.69	1.89	0.78
	5	0.026	0.84	0.028	0.68	1.26	1.33

The best fit conductivity values for vertical and horizontal polarization are now different, despite the fact that according to the specifications, the wall is structurally symmetric. These differences may be partly due to the fact that the measurement procedure involves angular variation in the horizontal plane. Therefore, as the incidence angle departs from normal, a wavefront with perpendicular polarization will "see" an increasing degree of shading by rods that are parallel to the electric field vector.

As before, only the theoretical curve for the single-ray model is shown. Table II allows the comparison of the modeling results for the two nominally equal concrete walls, as was described before for the case of brick walls. The results obtained again indicate that the choice of the value of ε_r is not critical. The range of values between 5 and 8 proved quite adequate. In contrast, the predicted attenuation is quite sensitive to the choice of σ. As discussed above, the measurements performed on wall 4 suggest a departure from homogeneous behavior, which translates into significant differences in the values of σ for each polarization. Applying the resulting models to wall 3 confirms this characteristic. Conversely, using wall 3 as a reference results in values of σ, which is quite close to those obtained for wall 4, and with a significantly larger value for vertical polarization. The large values of σ for these walls imply that both models (single-ray and multi-ray) yield virtually identical results.

For the walls considered, modeling error and average prediction error are less than 2 dB in most cases. They agree well with the results reported by other authors, contrasting prediction by analytical procedures with empirical data (see [8], [20], and [21], for example).

The lack of sensitivity of the models to the exact value of ε_r implies that the determination of a model based on equivalent parameters for a given wall type essentially requires the determination of σ. Measurements for a few incidence angles are easy to perform and can be repeated quickly at several positions and polarizations for representative walls. The resulting parameter values can then be compared with each other to verify consistency. In any practical situation, differences will exist, and average parameter values will have to be used in the prediction

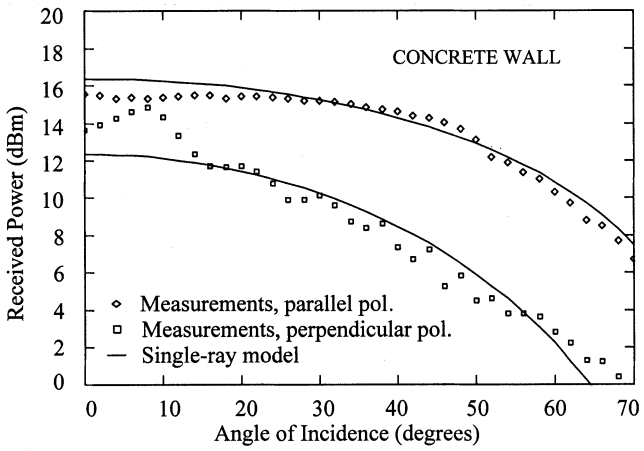

Fig. 7. Received power for reinforced concrete wall (wall 4).

model. The range of variation of the best fit values for σ will be an indication of the accuracy of the model.

The modeling procedure can thus be approached as follows. For a chosen adequate value of ε_r (the average of typical values for the corresponding wall type), σ can be determined by the following.

i) measurement of the total through-wall attenuation from which the power transmission coefficient (or its single-ray approximation $\tilde{T}$) easily deduced (For brick walls, measurements at normal incidence should be adequate, whereas for structures that show bigger nonhomogeneity, such as the described steel-reinforced concrete walls, a broader range of angles should be considered.);
ii) calculation of mismatch attenuation, i.e., T_{12}^2, of the imaginary lossless wall from (5) or (6);
iii) calculation of A^2 from (3), the attenuation coefficient α from (4), and the conductivity σ through (2).

The above analysis is based on the average of multiple measurements. The standard deviation of these measurements [see (10)] for a given wall and polarization will indicate the extent of

TABLE II
MODELING ACCURACY FOR CONCRETE WALL

		Wall 4 (reference)				Wall 3 (prediction errors)	
		Perpendicular		Parallel		Perpendicular	Parallel
Model	ε_r	σ (S/m)	$e_{r.m.s}$ (dB)	σ (S/m)	$e_{r.m.s}$ (dB)	$e_{r.m.s}$ (dB)	$e_{r.m.s}$ (dB)
Single-ray	5.5	0.092	1.29	0.070	0.49	2.21	0.87
	6.5	0.096	1.25	0.076	0.47	2.04	1.01
	7.5	0.102	1.27	0.080	0.53	2.14	0.94
Multi-ray	5.5	0.090	1.25	0.07	0.50	2.02	0.86
	6.5	0.096	1.26	0.076	0.47	2.04	0.97
	7.5	0.102	1.27	0.080	0.53	2.14	1.00

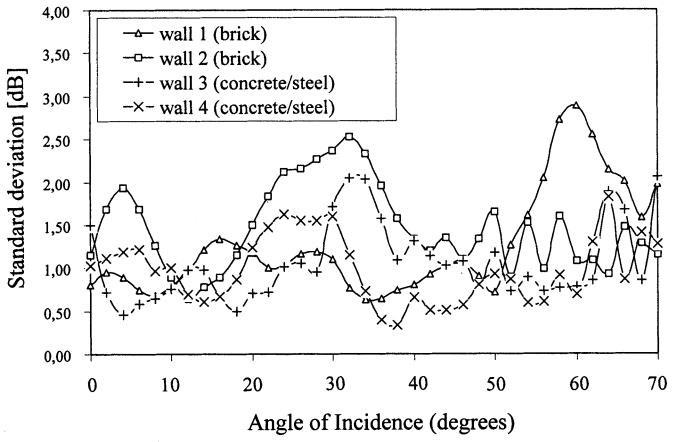

Fig. 8. Standard deviation of measurements for perpendicular polarization.

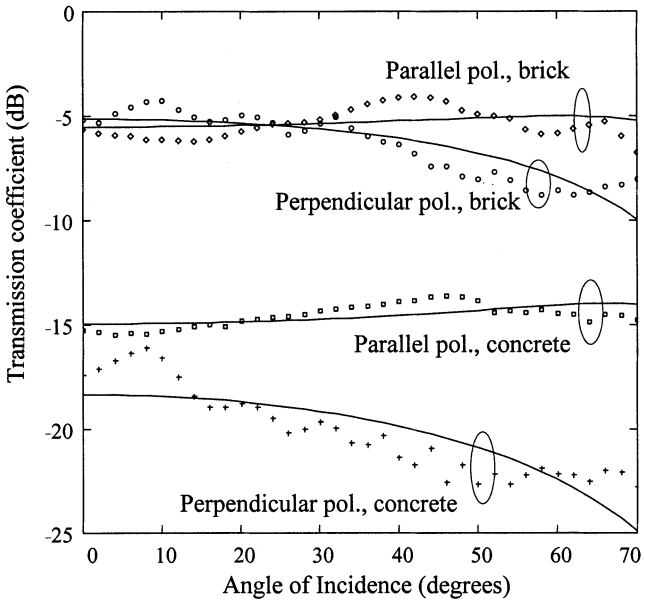

Fig. 9. Transmission coefficient, brick, and concrete walls. Model (solid lines) and measurements (dotted lines).

smoothing that results from the averaging procedure and, thus, the degree of nonhomogeneity. Fig. 8 shows the results obtained for perpendicular polarization for the brick and concrete walls as a function of angular position. There is no indication that the errors become larger at any particular range of incidence angles. Surprisingly, for a given polarization, the plots also show no evidence that the nonhomogeneity is larger for the reinforced concrete walls than for the brick walls. While the averaging process obviously smoothed the errors in the attenuation curves for all cases, there is no indication that the smoothing effect was more significant for the concrete walls.

Finally, we present in Fig. 9 a comparison of the transmission coefficients for one brick (wall 1) and one concrete wall (wall 4). The solid lines show in each case the predicted attenuation for the best fitting single-ray model, as tabulated before. The dotted lines represent the averaged measured values. The curves provide reference data for typical building walls.

As in all semi-empirical models, the proposed technique has its limitations, most notably the fact that for accurately determining the equivalent electric parameters, measurements have to be performed on walls that are representative for the buildings under consideration. In contrast, the more precise analytical or numerical methods are meant to use actual material and construction data. In practice, the internal wall structures are usually known for new buildings only, and even when this is the case, the validation of an exact numerical model will also involve measurements.

V. CONCLUSION

The through-wall attenuation, and the equivalent permittivity (ε) and conductivity (σ) of brick and concrete walls are estimated for the 900-MHz cellular band by a "best fit" of through-wall transmission measurements to the classical multi-ray model and its one-path approximation: the single-ray model. A measurement procedure and a laboratory setup are developed, and extensive experimental results confirming the validity of both models are presented.

It is numerically proven that the transmitted wave in lossy building walls is practically uniform, and the use of the classical ray-tracing theory for studying reflection and transmission phenomena is well justified.

The attenuation in brick walls and concrete building walls with two reinforcing steel meshes is studied. To our knowledge, no data has been explicitly given in the literature for the latter wall configuration.

The conclusion can be drawn that for brick and concrete walls, the single-ray model performs adequately for transmission, whereas for reflection the use of the more accurate multi-ray model would be more appropriate.

It is found that the permittivity can be chosen within a range of values that matches with those reported in the literature. The choice of the conductivity is critical for precise attenuation prediction. The measurements needed to determine the conductivity are simple and do not require complex equipment or extensive measurements. What is required basically is a noncoherent pulsed transmission and reception system to measure average loss at a few incidence angles.

Departures from homogeneous behavior can be expected for steel reinforced walls, leading to different model parameters, depending on polarization. This is, of course, expected if the geometrical arrangement of the vertical and horizontal reinforcement elements is different. Even for the symmetrical case, however, identical behavior for both polarizations would only be expected for normal incidence. For any other case, the influence of the conducting elements on the wave front will depend on whether or not the electrical field vector is parallel or perpendicular to the plane of incidence. This was confirmed by our measurements, which showed a consistent increase in the losses for the case of vertical polarization with respect to horizontal. On the other hand, for a given type of polarization, the presence of the steel meshes in the concrete walls did not generate larger measurement fluctuations than those observed in the inherently more homogeneous brick walls. Modeling error and average prediction error are found to be less than 2 dB in most cases. Typical r.m.s deviations of the measurements from their averages were found to be of the order of 1.5 dB over the angular range considered.

ACKNOWLEDGMENT

The authors wish to thank the anonymous reviewers and Dr. R. Valenzuela of Bell Laboratories, Lucent Technologies for their valuable criticism and suggestions.

REFERENCES

[1] W. Honcharenko and H. L. Bertoni, "Transmission and reflection characteristics at concrete block walls in the UHF bands proposed for future PCS," *IEEE Trans. Antennas Propagat.*, vol. 42, pp. 232–239, Feb. 1994.

[2] R. Dalke, C. L. Holloway, and P. McKenna, "Reflection and transmission properties of reinforced concrete walls," in *Proc. IEEE Antennas Propagat. Soc. Int. Symp. Dig.*, July 1999, pp. 1502–1505.

[3] E. Richalot, M. Bonilla, M.-F. Wong, V. Fuad-Hanna, H. Baudrand, and J. Wiart, "Electromagnetic propagation into reinforced-concrete walls," *IEEE Trans. Microwave Theory Tech.*, vol. 48, pp. 357–366, Mar. 2000.

[4] *Tools for Wireless Design, MCS™ 3.0, Software Product Catalog*, EDX Eng., Inc., 1998.

[5] *WiSE – A Wireless System Engineering Tool*, Bell Labs.-Lucent Technol.

[6] R. P. Torres, L. Valle, M. Domingo, and M. C. Diez, "CINDOOR: An engineering tool for planning and design of wireless systems in enclosed spaces," *IEEE Antennas Propagat. Mag.*, vol. 41, pp. 11–2, Aug. 1999.

[7] S. Y. Seidel and T. S. Rappaport, "Site-specific propagation prediction for wireless in-building personal communication system design," *IEEE Trans. Veh. Technol.*, vol. 43, pp. 879–891, Nov. 1994.

[8] O. Landron, M. J. Feuerstein, and T. S. Rappaport, "A comparison of theoretical and empirical reflection coefficients for typical exterior wall surfaces in a mobile radio environment," *IEEE Trans. Antennas Propagat.*, vol. 44, pp. 341–350, Mar. 1996.

[9] E. Zollinger, "Indoor wave propagation and analysis techniques, IEEE MTT-S Int. microwave symposium," in *Proc. Workshop WMFG Papers Field Theoretical Problems Wireless Technol.*, Orlando, FL, May 1995.

[10] C. F. Yang, C. J. Ko, and B. C. Wu, "A free space approach for extracting the equivalent dielectric constants of the walls in buildings," in *Proc. IEEE Antennas Propagat. Soc. Int. Symp. Dig.*, July 1999.

[11] H. Leaderman and L. A. Turner, *Theory of the Reflection and Transmission of Electromagnetic Waves by Dielectric Materials*. New York: McGraw-Hill, 1948, vol. 26, MIT Rad. Lab. Series.

[12] W. D. Burnside and K. W. Burgener, "High frequency scattering by a thin lossless dielectric slab," *IEEE Trans. Antennas Propagat.*, vol. AP-31, pp. 104–110, Jan. 1983.

[13] C. A. Balanis, "Refraction of a uniform plane wave on a plane boundary between two lossy media," *IEEE Trans. Antennas Propagat.*, vol. AP-26, pp. 738–741, Sept. 1978.

[14] Y. Wang, S. Safavi-Naeni, and S. K. Chaudhuri, "A hybrid techniques based on combining ray tracing and FDTD methods for site-specific modeling of indoor radio wave propagation," *IEEE Trans. Antennas Propagat.*, vol. 48, pp. 743–754, May 2000.

[15] E. C. Jordan and K. G. Balmain, *Electromagnetic Waves and Radiating Systems*. Englewood Cliffs, NJ: Prentice-Hall, 1968.

[16] S. Y. Tan and H. S. Tan, "A microcellular communication propagation model based on the uniform theory of diffraction and multiple image theory," *IEEE Trans. Antennas Propagat.*, vol. 44, pp. 341–350, Oct. 1996.

[17] C. L. Holloway, P. L. Perini, R. R. DeLyser, and K. C. Allen, "Analysis of composite walls and their effects on short-path propagation modeling," *IEEE Trans. Veh. Technol.*, vol. 46, pp. 730–735, Aug. 1997.

[18] J. H. Tarng and T. R. Liu, "Effective models in evaluating radio coverage on single floors of multifloor buildings," *IEEE Trans. Veh. Technol.*, vol. 48, pp. 782–789, May 1999.

[19] V. Erceg, S. Ghassenzadeh, M. Taylor, D. Li, and D. Schilling, "Urban suburban out-of-site propagation modeling," *IEEE Commun. Mag.*, vol. 30, pp. 56–61, June 1992.

[20] "Digital Mobile Radio Toward Future Generation Systems," EC/COST Telecommunications, Brussels, Belgium, COST 231 Final Report, COST Action 231, 1999.

[21] H. Bertoni, *Radio Propagation for Modern Wireless Systems*. Englewood Cliffs, NJ: Prentice-Hall PTR, 2000, ch. 3.

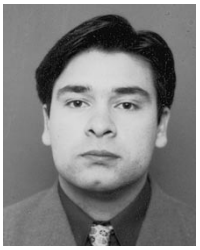

Daniel Peña received the Ingeniero Civil Electrónico and Magister en Electrónica degrees from the Universidad Técnica Federico Santa María, Valparaiso, Chile, in 2000.

He has been a Systems Engineer with Siemens Chile since August 2000 and is a Cisco Certified Network Associate. His interests include data communications and wireless systems.

Rodolfo Feick (SM'94) received the Ingeniero Civil Electrónico degree from the Universidad Técnica Federico Santa María, Valparaiso, Chile, in 1970 and the M.Sc. and Ph.D. degrees in electrical engineering from the University of Pittsburgh, Pittsburgh, PA, in 1972 and 1975, respectively.

He has been with the Department of Electronics Engineering, Universidad Técnica Federico Santa María, since 1975. His interests include wireless systems and data communications.

Hristo D. Hristov (SM'87) received the Ph.D. and D.Sc. degrees in wireless communications from the Technical University, Sofia, Bulgaria.

Since 1965, he has been with the Technical University of Varna, Varna, Bulgaria, and currently, he is a Visiting Research Professor with the Universidad Técnica Federico Santa María, Valparaiso, Chile. His current research interests include high-frequency electromagnetics, antennas, passive microwave and quasioptical devices, and mobile wireless communications. He was a research fellow at the Strathclyde University of Technology, Glasgow, U.K.; Queen Mary College, London, U.K.; and at Eindhoven University of Technology, Eindhoven, the Netherlands. He was also a Visiting Professor at the Electrotechnical University, St. Petersburg, Russia; National Technical University of Athens, Athens, Greece; Tsukuba University, Tsukuba, Japan; Aalborg University Center, Aalborg, Denmark; and Lyngby National Technical University, Lyngby, Denmark. He is the co-author of *Microwave Cavity Antennas* (Norwood, MA: Artech House: 1989) and the author of *Fresnel Zones in Wireless Links, Zone Plate Lenses and Antennas* (Norwood, MA: Artech House: 2000).

Dr. Hristov participated as an observer-expert in the COST-245 and COST-260 European research projects on antennas for satellite and mobile communications. He was an invited lecturer at the Tokyo AP-S Chapter, the Sweden AP-S/MTT-S Chapter, and the ESA/ESTEC, the Netherlands. He served as an organizer and chair of the Bulgarian IEEE Section and MTT/AP-S Chapter. He was awarded the IEEE Third Millenium Medal.

Walter Grote received the Ingeniero Civil Electrónico degree from Universidad Técnica Federico Santa María, Valparaiso, Chile, in 1975 and the M.Sc. and Ph.D. degrees in electrical engineering from Polytechnic University, Brooklyn, NY, in 1984 and 1992, respectively.

He has been with the Department of Electronics Engineering, Universidad Técnica Federico Santa María, since 1975. His interests include wireless systems and data communications.